

N74-14610

CRACKED FINITE ELEMENTS PROPOSED FOR NASTRAN

By J. A. Aberson, The Lockheed-Georgia Company
and J. M. Anderson, Georgia Institute of Technology

SUMMARY

The recent introduction of special crack-tip singularity elements, usually referred to as cracked elements, has brought the power and flexibility of the finite-element method to bear much more effectively on fracture mechanics problems. This paper recalls the development of two cracked elements and presents the results of some applications proving their accuracy and economy. Judging from the available literature on numerical methods in fracture mechanics, it seems clear that the elements described have been used more extensively than any others in practical fracture mechanics applications.

INTRODUCTION

The study of crack growth behavior by classical continuum linear fracture mechanics has been limited primarily to simple structural configurations and loadings. Because of the ease with which the finite-element method handles discontinuous loads and boundary conditions, attempts have been made to use this method to study fracture in complex structures. The capability of conventional elements and conventional modeling procedures to predict crack-tip parameters accurately has been found to be limited and uneconomical. The most significant and accurate results obtained through use of standard methods are those which follow the work reported by Chan et. al. (ref. 1) and Kobayashi et. al. (ref. 2). The method followed by Kobayashi, for example, is to use the crack-opening displacements to solve a sequence of two simultaneous equations relating displacements to the two stress-intensity factors, K_I and K_{II} , for the opening and sliding fracture modes, respectively. These results are then interpreted or extrapolated to predict values at the crack tip. The difficulty in applying this approach lies in trying to accurately depict the extreme stress gradient existing in the near vicinity of a crack tip. The detail required for a model to reasonably characterize this gradient makes the procedure expensive and cumbersome. For example, Oglesby and Lomacky (ref. 3) indicate that the maximum permissible element size necessary to insure acceptable accuracy in the computed stress-intensity factors is of the order of 1/300th of the crack half-length. To achieve detail of this order, substructure analyses have usually been used. That is, a coarse model is first analyzed to obtain boundary conditions which are then imposed on a more refined local model of the crack region. In some instances results from the second model have been used to analyze a third and even more finely modeled localized region of the crack tip. Obviously, considerable modeling and computer efforts are necessary to carry out such analyses.

Another approach, which is similar to that used by Chan and Kobayashi, is a combination of finite-element and boundary-collocation analyses. In this method, displacements and stresses from a conventional finite element model - which may or may not contain some representation of a crack - are used as boundary points in a boundary collocation solution for the crack. This is the procedure followed by Freese and Kaldjian (ref. 4), for example. The disadvantage of this combined approach is that it is not easily applicable since considerable experience in fracture analysis and complex variables is required to obtain consistently accurate results.

In an attempt to circumvent the economic problem of the conventional approach and the applicability problem of the combined approach, research and development efforts have been turned toward formulating elements which are capable of characterizing the crack-tip stress singularity internally. These singularity elements - cracked finite elements - provide a new means for computing stress-intensity factors and thereby predicting crack growth. Two such elements have been developed and implemented at the Lockheed-Georgia Company. These elements have received extensive usage in project and contract work and have provided considerable substantiation of the accuracy of the approach used in their formulation. A description of the formulation and implementation of these elements follows.

TECHNICAL DEVELOPMENT

The Williams' series of stress functions (refs. 5 and 6)* is the basis for all boundary collocation and cracked finite-element schemes to estimate stress-intensity factors. This series gives the following familiar expressions for the in-plane stresses for the plane crack problem illustrated in figure 1.

$$\begin{aligned}
 \sigma_r(r, \theta) &= \sum_{n=1}^{\infty} \frac{n}{4} \cdot r^{\frac{n}{2}-1} \left\{ s_n \left[-(n+2) \cos \left(\frac{n}{2} + 1 \right) \theta + f(n)(n-6) \cos \left(\frac{n}{2} - 1 \right) \theta \right] \right. \\
 &\quad \left. + a_n \left[g(n)(n+2) \sin \left(\frac{n}{2} + 1 \right) \theta - (n-6) \sin \left(\frac{n}{2} - 1 \right) \theta \right] \right\} \\
 \sigma_{\theta}(r, \theta) &= \sum_{n=1}^{\infty} \frac{n}{4} (n+2) r^{\frac{n}{2}-1} \left\{ s_n \left[\cos \left(\frac{n}{2} + 1 \right) \theta - f(n) \cos \left(\frac{n}{2} - 1 \right) \theta \right] \right. \\
 &\quad \left. + a_n \left[-g(n) \sin \left(\frac{n}{2} + 1 \right) \theta + \sin \left(\frac{n}{2} - 1 \right) \theta \right] \right\} \tag{1}
 \end{aligned}$$

* An error in reference 5 was subsequently corrected by Williams in reference 6.

and

$$\tau_{r\theta}(r, \theta) = \sum_{n=1}^{\infty} \frac{n}{4} r^{\frac{n}{2}-1} \left\{ s_n \left[(n+2) \sin \left(\frac{n}{2} + 1 \right) \theta - f(n)(n-2) \sin \left(\frac{n}{2} - 1 \right) \theta \right] \right. \\ \left. + a_n \left[g(n)(n+2) \cos \left(\frac{n}{2} + 1 \right) \theta - (n-2) \cos \left(\frac{n}{2} - 1 \right) \theta \right] \right\}$$

in which

$$f(n) = \frac{\frac{n}{2} + 1}{\frac{n}{2} + (-1)^n}$$

and

$$g(n) = \frac{\frac{n}{2} - (-1)^n}{\frac{n}{2} + 1}$$

(2)

The independent constants associated with the symmetric (even in θ) and anti-symmetric (odd in θ) parts of the Williams' series have been denoted in equation (1) by s_n and a_n , respectively. Even though an expression for the second antisymmetric term has been formally written, it should be noted before proceeding that it never contributes to any of the stresses. Thus in the usual finite-element description, a_2 is not a legitimate generalized coordinate.

The leading terms in equation (1) are singular like $r^{-1/2}$; all subsequent terms are nonsingular. The coefficients s_1 and a_1 are related to the opening and sliding mode stress-intensity factors K_I and K_{II} by the following formulas:

$$\left. \begin{aligned} K_I &= \lim_{r \rightarrow 0} \sqrt{2\pi r} \sigma_{\theta}(r, 0) = 3 \sqrt{2\pi} s_1 \\ K_{II} &= \lim_{r \rightarrow 0} \sqrt{2\pi r} \tau_{r\theta}(r, 0) = \sqrt{2\pi} a_1 \end{aligned} \right\} \quad (3)$$

The strains corresponding to the stresses in equation (1) are obtained through Hooke's law. The strain-displacement equations in plane polar coordinates can then be integrated for the radial and tangential displacement components $u_r(r, \theta)$ and $u_{\theta}(r, \theta)$, respectively. See, for example, reference 7 and the subsequent correction. The resulting displacement components are

$$\begin{aligned}
u_r(r, \theta) &= K \cos \theta + H \sin \theta \\
&+ \sum_{n=1}^{\infty} \frac{1}{4G} r^{\frac{n}{2}} \left\{ s_n \left[-(n+2) \cos \left(\frac{n}{2} + 1 \right) \theta - f(n)(6-8\sigma-n) \cos \left(\frac{n}{2} - 1 \right) \theta \right] \right. \\
&\left. + a_n \left[(n+2) g(n) \sin \left(\frac{n}{2} + 1 \right) \theta + (6-8\sigma-n) \sin \left(\frac{n}{2} - 1 \right) \theta \right] \right\} \quad (4)
\end{aligned}$$

and

$$\begin{aligned}
u_\theta(r, \theta) &= Fr + H \cos \theta - K \sin \theta \\
&+ \sum_{n=1}^{\infty} \frac{1}{4G} r^{\frac{n}{2}} \left\{ s_n \left[(n+2) \sin \left(\frac{n}{2} + 1 \right) \theta - f(n)(6-8\sigma+n) \sin \left(\frac{n}{2} - 1 \right) \theta \right] \right. \\
&\left. + a_n \left[(n+2) g(n) \cos \left(\frac{n}{2} + 1 \right) \theta - (6-8\sigma+n) \cos \left(\frac{n}{2} - 1 \right) \theta \right] \right\}
\end{aligned}$$

in which F, H, and K are rigid-body displacement parameters and G is the shear modulus. The dimensionless elastic constant σ is given by

$$\sigma = \begin{cases} \nu & \text{(for plane strain)} \\ \frac{\nu}{1+\nu} & \text{(for plane stress)} \end{cases}$$

where ν is Poisson's ratio.

Most cracked finite elements developed to date (c.f. refs. 8-11) incorporate only the leading symmetric terms in equations (1) and (4). Creager, at the Lockheed-California Company in 1970, attempted to include subsequent terms in the Williams' series but was unsuccessful due to inadequate element geometry. This was successfully accomplished by Wilson (ref. 12) with a symmetric element, which makes use of the first four terms. Wilson's element, however, has the disadvantage of being semicircular and, hence, is awkward to use in conjunction with conventional elements which almost always have straight boundaries. Moreover, the Wilson element (as well as some others previously referenced) has fewer degrees of freedom than are needed for independence of the nodal displacements. At best this requires that the stiffness matrix of the cracked element receive special attention in forming the stiffness matrix of the assembly.

At Lockheed-Georgia, the decision was made at the outset to develop a cracked finite element that is a high-order element in that it

- (i) incorporates many of the terms in the Williams' series;
- (ii) has a perfect balance between actual degrees of freedom and number of nodal displacements; and
- (iii) has a convenient shape for interfacing with conventional elements.

The first feature permits accurate estimates of stress-intensity factors with relatively coarse finite-element grids, while the second and third features allow the numerical analyst to add the cracked element to an assembly in the same way that he adds a conventional element.

Because many fracture mechanics problems are symmetric about the plane of the crack, two elements were developed at Lockheed-Georgia. One takes only the symmetric terms in the Williams' series and, hence, is applicable only to symmetric problems ($K_{II} = 0$); the other makes use of both symmetric and anti-symmetric terms and is applicable to unsymmetric or mixed mode (K_I and K_{II}) problems.

Plane-Deformation Symmetric Element

Figure 2 shows the eight-node-symmetric element. The elemental coordinate system has its origin at the crack tip. The element is rectangular with a three-to-one aspect ratio. Placement of the nodes relative to the rectangle is pre-determined with a node at each corner plus nodes at the one-third points of each of the long sides. The choice of the symmetric element's shape - three equal squares - was considered convenient since the use of regular mesh spacings is common in finite-element models. This geometry has also proven to be effective when used with constant-strain triangles. The lower side (nodes 6, 7, 8, and 1) is coincident with the crack direction and presumed axis of symmetry. Nodes 6 and 7 are on the free crack face. Nodes 8 and 1 are on the prolongation of the crack. They are constrained rigidly as to vertical displacement and are free of shear forces - conditions consistent with symmetry.

The element has sixteen displacement degrees of freedom - two per node corresponding to the in-plane displacement components. Thus, in keeping with feature (ii) mentioned previously, it incorporates the first thirteen symmetric terms of the Williams' series plus the three displacement degrees of freedom associated with rigid-body displacement in the plane. In the following, the thirteen Williams' coefficients and the three rigid-body parameters are referred to as the sixteen generalized coordinates of the element. The stresses and displacements corresponding to these sixteen generalized coordinates are evaluated on the boundary of the element. Products of stress and displacement contributing to boundary work are formed and integrated. The result is a homogeneous quadratic form in the generalized coordinates, and the coefficient of each term is an element of the cracked element's stiffness matrix with respect to the generalized coordinates.

Once the stiffness matrix relative to generalized coordinates is determined, the stiffness matrix relative to nodal displacements is formed using equation (4).

To date this element has not failed to substantiate any reliable stress-intensity factor to within 2% difference. And more often than not, this was accomplished with a relatively coarse finite-element grid. Results obtained with the symmetric element will be discussed later in the section "Applications."

Plane-Deformation Unsymmetric Element

The ten-node unsymmetric element is shown in figure 3. The element is square with equally spaced nodes around its boundary. As before, the shape (4 equal squares) and relative location of the nodes are fixed, and were chosen to provide modeling convenience. Again, the actual size of the element and its elastic constants dictated by the particular application are input parameters. The generalized coordinates correspond to the first nine symmetric terms and first eight antisymmetric terms of the Williams' series plus the three rigid-body displacement parameters. The stiffness matrix was again generated by integration around the boundary.

Results obtained with this element are presented in the following section. Although sufficient, the accuracy obtained with this unsymmetric element is not as impressive as that obtained with the symmetric element previously discussed. This is understandable in light of the fact that the unsymmetric element has fewer degrees of freedom that it can bring to bear on each mode. Of course, it can be used in a much wider class of crack problems and is more practical for industrial applications. In the following section some examples are given which show the accuracy and applicabilities of both the symmetric and unsymmetric elements.

APPLICATIONS

To illustrate the capabilities of the two elements, four examples of their usage follow. These examples were chosen to demonstrate first, the accuracy and economy of the elements and second, the capacities of the elements to perform analyses for structural configurations of practical importance. The four cases are drawn from a wide range of work involving use of the cracked elements and represent typical rather than most favorable results.

The cracked elements are implemented in a standard single-precision finite-element displacement-method program which employs a banded Cholesky decomposition solution procedure. This program, which operates on a Univac 1106 computer, was used for all four examples.

Case 1: Symmetric-Element Test Case

This example, shown on figure 4, was one of the first analyzed with the symmetric element. However, it exhibits the degree of accuracy which has been consistently achieved in numerous subsequent problems. The finite-element model has 31 nodes, 35 constant-strain triangles, and 1 eight-node cracked

element. The three configurations of single-edge crack, double-edge crack and center crack were all individually analyzed with this one model for an a/w ratio of 1/3. The model grid, which is quite coarse, results in the single-edge crack model having 57 displacement degrees of freedom (DOF) while the double-edge and center models have 51 DOF each. Comparisons of the stress-intensity factors computed using these configurations with ASTM values are shown on figure 4. The accuracy of the finite-element predictions are impressive ($\leq 1.5\%$ error) for all three cases. Computer time to perform each analysis was 3 to 4 seconds.

Subsequent work with this finite-element model and others like it showed comparable results, with refinements in the grid bringing steady convergence toward ASTM values.

Case 2: Symmetric Cracked Hole

The symmetric problem depicted in figure 5 was analyzed in order to assess the accuracy of the formula

$$K_I = \beta_{\text{Bowie}} \beta_{\text{Isida}} \sigma \sqrt{\pi a} \quad (5)$$

which is routinely used to estimate stress-intensity factors for this geometry. In equation (5) β_{Bowie} and β_{Isida} are the correction factors, respectively, associated with Bowie's (ref. 13) analysis for the presence of the hole and Isida's (ref. 14) analysis for the finite-width effect. The finite-element grid as shown in figure 5 was established (i) to permit the location of the cracked element to be easily changed to simulate growth of the symmetric crack, and (ii) to permit the width of the plate to be readily changed by removing columns of constant-strain triangular elements from the right edge. The stress-intensity factors computed in this parametric study are listed in table 1. An important conclusion to be drawn from these results is that the value predicted by equation (5) seems adequate for short cracks, but becomes quite inaccurate and nonconservative as the crack grows long.

Such parametric analyses are of practical value, however, only if they can be quickly and economically accomplished. The use of the symmetric cracked element made it possible for a relatively coarse model (figure 5) to give accurate answers. The analysis of this coarse model required 28 000 words of computer storage and approximately 20 seconds of computer time. The total study, which includes model conception, data input, and 21 separate analyses, required less than 1 man-day of engineering effort and 7 minutes of computer time. Subsequent studies of other parameters, e.g. fastener loads or fastener interference, could now be accomplished with even less effort since the model can be saved and reused.

In general, the computer times and storage cited above are economical, and, in addition, are well within the operational limits of most remote access or time-sharing computer facilities. This economy and ready availability in a

remote access mode (Univac DEMAND) have resulted in widespread application of cracked elements at the Lockheed-Georgia Company in studies such as the one described above.

Case 3: Pin-Loaded Lug

The structural member shown on figure 6 is a lug and occurs frequently in aerospace structures. The lug's lack of geometric symmetry greatly hampers the use of approximate methods to adequately estimate its stress-intensity factors K_I and K_{II} when a crack appears. Such cracked geometry is easily handled, however, with the unsymmetric cracked element. The lug and the pin loading it are modeled with constant-strain triangles and a cracked element as shown on figure 7. The unsymmetric cracked element is shown in its initial position. As in the previous example, the model grid was constructed to permit the position of the cracked element to be easily changed to simulate the growth of the crack. Results of the analyses are given in Table 2. The small value of K_{II} relative to K_I for the initial position indicates that the behavior of the crack is primarily mode I or opening mode from the beginning. Figure 8 depicts the mode I behavior as the crack progresses from the hole to the outer edge.

This analysis, which is considered to be in error by less than 3 percent, was accomplished at the cost of 1 man-day and 4 minutes of computer time in 35 000 words of computer storage.

Case 4: 45-Degree Slanted Crack Test Specimen

This last example demonstrates the use of cracked elements to calibrate test configurations for accurate reduction of test data. The specimen shown by figure 9 contained an initial 45° center crack, and was subjected to a constant-amplitude tension-tension load. The maximum tension to minimum tension ratio was 0.1. The specimen was modeled with constant-strain triangles and an unsymmetric cracked element as shown by figure 10. The path taken by the crack during the cyclic test was simply traced on the finite-element model. The center section of the model was reconstructed seven times to accommodate the cracked elements for dimensionless projected crack lengths $\lambda = a/w$ of 0.3, 0.35, 0.4, 0.5, 0.6, 0.7, and 0.8. The steel loading pins for the test were modeled by spring elements spread over the approximate bearing surfaces as shown.

The results from the analyses of this model are shown on figure 11. The curves on figure 11 are considered accurate within 2 percent. These results show an interesting and potentially significant feature not found in similar work reported by Iida and Kobayashi (ref. 15). For $0.5 \leq \lambda \leq 0.75$ the mode I stress-intensity factor K_I is greater than K_I for a straight crack of the same projected length. This increase in K_I (the "hump" in figure 11) occurs when K_{II} goes to zero and could easily account for the increased crack-growth rates observed for this type of specimen. However, the significant point to this analysis is that an accurate knowledge of K_I and K_{II} for test articles permits

a concise reduction of crack-growth-rate data for later design usage.

The analysis of this case required approximately 80 seconds of computer time for each configuration. The total for all seven configurations, including data input and modifications, was 9.4 minutes.

CONCLUSIONS

The incorporation into NASTRAN and other finite element codes of cracked elements appears to be both a timely and practical effort, for there is a growing concern among those involved in aerospace design with being able to perform reliable fracture analyses of damaged or flawed structures. This concern arises partly from anticipation of difficulties of meeting certain design "fracture criteria" imposed by procuring agencies for new aerospace vehicles and partly from recent experiences with existing airplanes. For whatever reasons, the fact is that fracture mechanics and fracture analyses have become significant and necessary steps in the design and modifications of aerospace structures. Thus, there is a pressing need for accurate production analysis tools to enable designers to apply new fracture criteria. Cracked finite elements, such as those discussed in this paper, are such tools. Their ease of application makes it possible for analysts and designers not extensively trained in fracture mechanics but familiar with finite element methods to compute accurate stress-intensity factors.

REFERENCES

1. Chan, S. K., Tuba, I. S., and Wilson, W. K.: On the Finite Element Method in Linear Fracture Mechanics. *Engineering Fracture Mechanics*, 2, 1970, pp. 1-17.
2. Kobayashi, A. S., Maiden, D. E., Simon, B. J., and Iida, S: Application of the Method of Finite Element Analysis to Two-Dimensional Problems in Fracture Mechanics. University of Washington, Department of Mechanical Engineering, ONR Contract Nonr-4/7(39), NR 064 478, TR No. 5, Oct. 1968.
3. Oglesby, J. J., and Lomacky, O.: An Evaluation of Finite Element Methods for the Computation of Elastic Stress Intensity Factors. Navy Ship Research and Development Center, NAVSHIPS Project SF 35.422.210, Task 15055, Report Number 3751, December 1971.
4. Freese, C. E., and Kaldjian, M. J.: Collocation and Finite Elements for Crack Analysis. Proceedings of the 13th Annual Symposium: Fracture and Flaws, University of New Mexico College of Engineering, March 1973.
5. Williams, M. L.: On the Stress Distribution at the Base of a Stationary Crack. *Journal of Applied Mechanics*, Vol. 24, No. 1, March 1957, pp. 109-114.

6. Williams, M. L.: Stress Singularities Resulting from Various Boundary Conditions in Angular Corners of Plates in Extension. *Journal of Applied Mechanics*, Vol. 74, December 1952, pp. 526-528.
7. Gross, B., Roberts, E., and Srawley, J. E.: Elastic Displacements for Various Edge-Cracked Plate Specimens. *Internat. J. Fracture Mechanics*, vol. 4, no. 3, Sept. 1968. Also errata, *Internat. J. Fracture Mechanics*, vol. 6, 1970.
8. Byskov, E.: The Calculation of Stress Intensity Factors Using the Finite Element Method with Cracked Elements. *International Journal of Fracture Mechanics*, Vol. 6, No. 2, June 1970, pp. 159-167.
9. Tracey, D. M.: Finite Elements for Determination of Crack Tip Elastic Stress Intensity Factors. *Engineering Fracture Mechanics*, Vol. 3, 1971, pp. 255-265.
10. Walsh, P. F.: The Computation of Stress Intensity Factors by a Special Finite Element Technique. *International Journal of Solids and Structures*, Vol. 7, 1971, pp. 1333-1342.
11. Pian, T. H. H., Tong, P., and Luk, C. H.: Elastic Crack Analysis by a Finite Element Hybrid Method. AFOSR-TR-72-0752, U.S. Air Force, Dec. 1971. (Available from DDC as AD 739 988.)
12. Wilson, W. K.: Crack Tip Finite Elements for Plane Elasticity. Westinghouse Research Laboratories Scientific Paper 71-1E7, FMPWR-P2, June 1971.
13. Bowie, O. L.: Analysis of an Infinite Plate Containing Radial Cracks Originating from the Boundary of an Internal Circular Hole. *Journal of Mathematics and Physics*, Vol. 35, 1956.
14. Isida, M.: On the Tension of a Strip with a Central Elliptical Hole. *Transactions, Japanese Society of Mechanical Engineers*, Vol. 22, 1956.
15. Iida, S., and Kobayashi, A. S.: Crack Propagation Rate in 7075-T6 Plates Under Cyclic Tensile and Transverse Shear Loadings. *Journal of Basic Engineering, Transactions ASME, Series D*, Vol. 91, No. 4, Dec. 1969, pp. 764-769.

Table 1. A Study of Finite-Width Panel with Two Symmetric Cracks Coming From a Hole

$\frac{W}{r}$	$\frac{a}{r}$	β (ISIDA)	β (BOWIE)	$\frac{K_I [\text{FROM EQ. (5)}]}{\alpha/\pi a}$	$\frac{K_I [\text{ELEMENT}]}{\alpha/\pi a}$	% DIFFERENCE
	0.3	1.02	2.15	2.19	2.18	-0.46
	1.9	1.08	1.23	1.33	1.42	6.33
8.0	3.5	1.25	1.12	1.40	1.52	7.89
	5.1	1.61	1.07	1.72	1.90	9.47
	6.7	3.14	1.05	3.29	4.08	19.36
	0.3	1.02	2.15	2.19	2.19	0.0
	1.5	1.10	1.29	1.42	1.47	3.40
6.4	2.7	1.27	1.16	1.48	1.53	3.27
	3.9	1.61	1.11	1.78	1.87	4.81
	5.1	3.01	1.07	3.21	3.96	18.94
	0.3	1.04	2.15	2.25	2.23	0.0
	1.1	1.13	1.42	1.61	1.62	0.62
4.8	1.9	1.31	1.23	1.62	1.64	1.22
	2.7	1.63	1.16	1.89	1.99	5.03
	3.5	2.89	1.12	3.24	3.57	9.24
	0.3	1.11	2.15	2.39	2.42	1.24
	0.7	1.21	1.64	1.99	2.01	1.00
3.2	1.1	1.39	1.42	1.97	2.02	2.48
	1.5	1.65	1.29	2.13	2.29	6.99
	1.9	2.40	1.23	2.95	3.25	9.23
1.6	0.3	1.873	2.15	4.01	4.46	10.09

Table 2. Results from Analysis of the Lug Model

$\frac{a}{r}$	$\frac{K_I}{\sigma_B \sqrt{\pi a}}$	$\frac{K_{II}}{\sigma_B \sqrt{\pi a}}$
0.1112	2.770	0.123
0.3335	1.796	-0.002
0.5559	1.586	0.004
0.7782	1.775	0.004

crack length = a

hole radius = r

mean bearing stress = σ_B

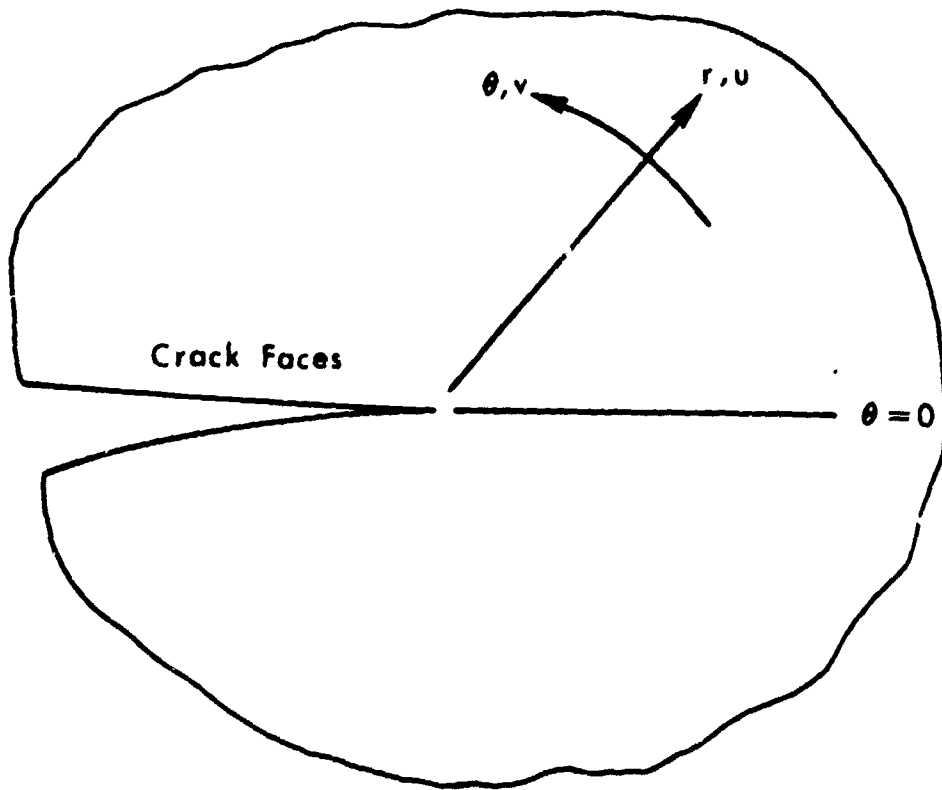


Figure 1. - Neighborhood around a crack tip.

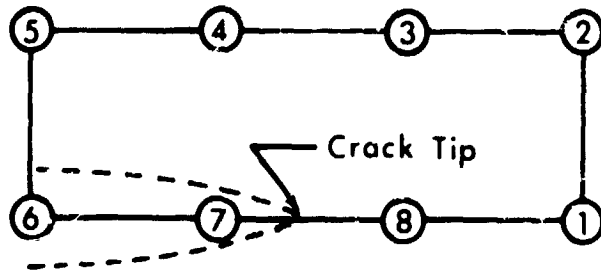


Figure 2.- Eight-node element for symmetric problems.

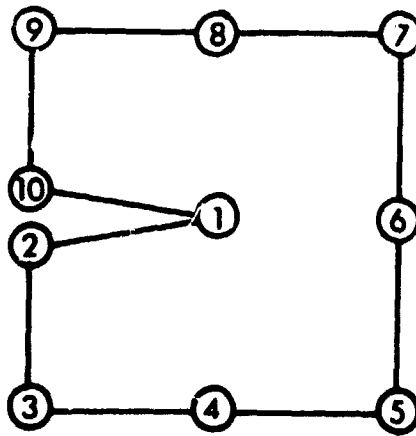


Figure 3.- Ten-node element for unsymmetric problems.

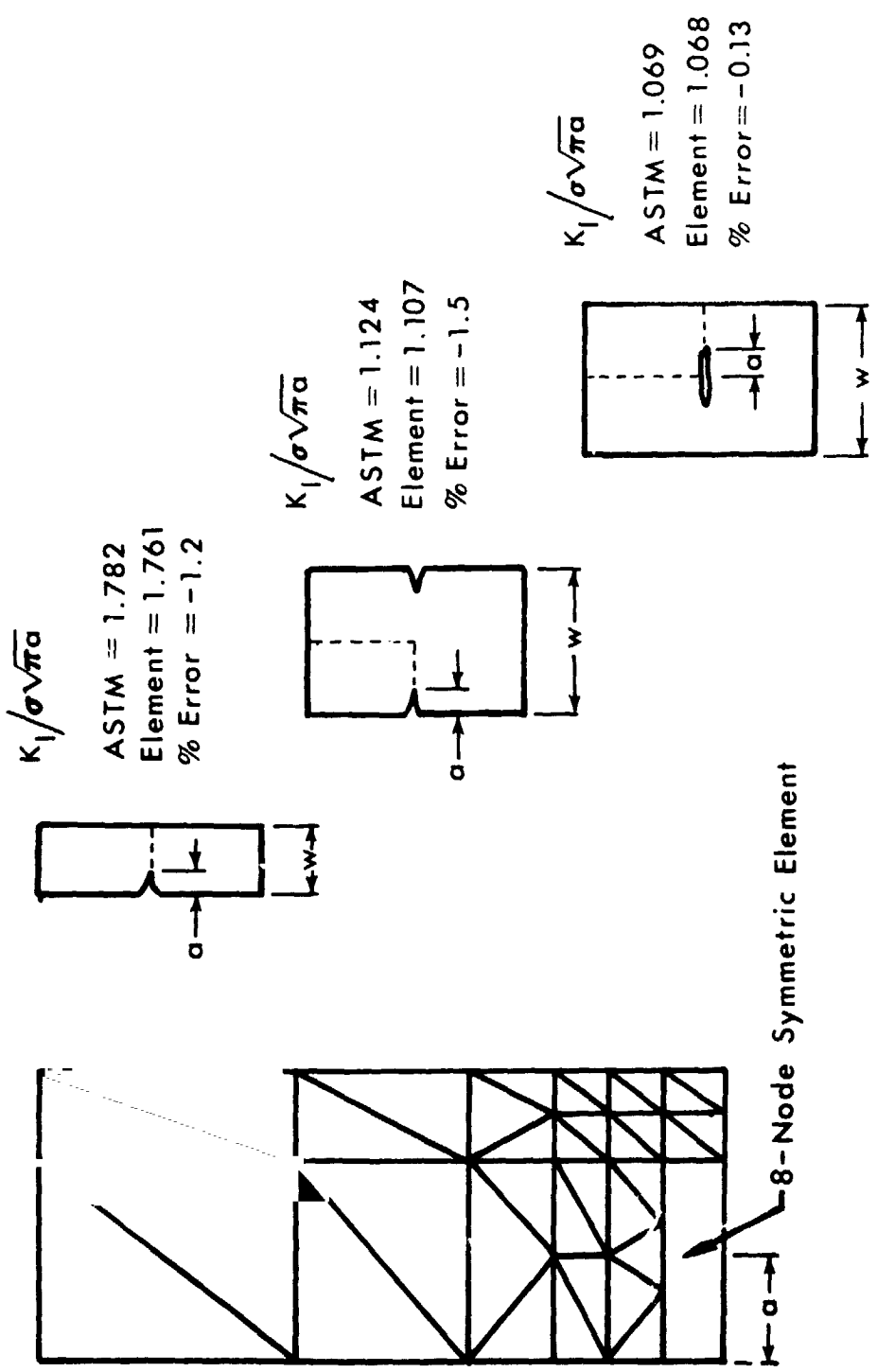


Figure 4. - Results for single-edge, double-edge, and center cracked tension panels with $a/w = 1/3$.

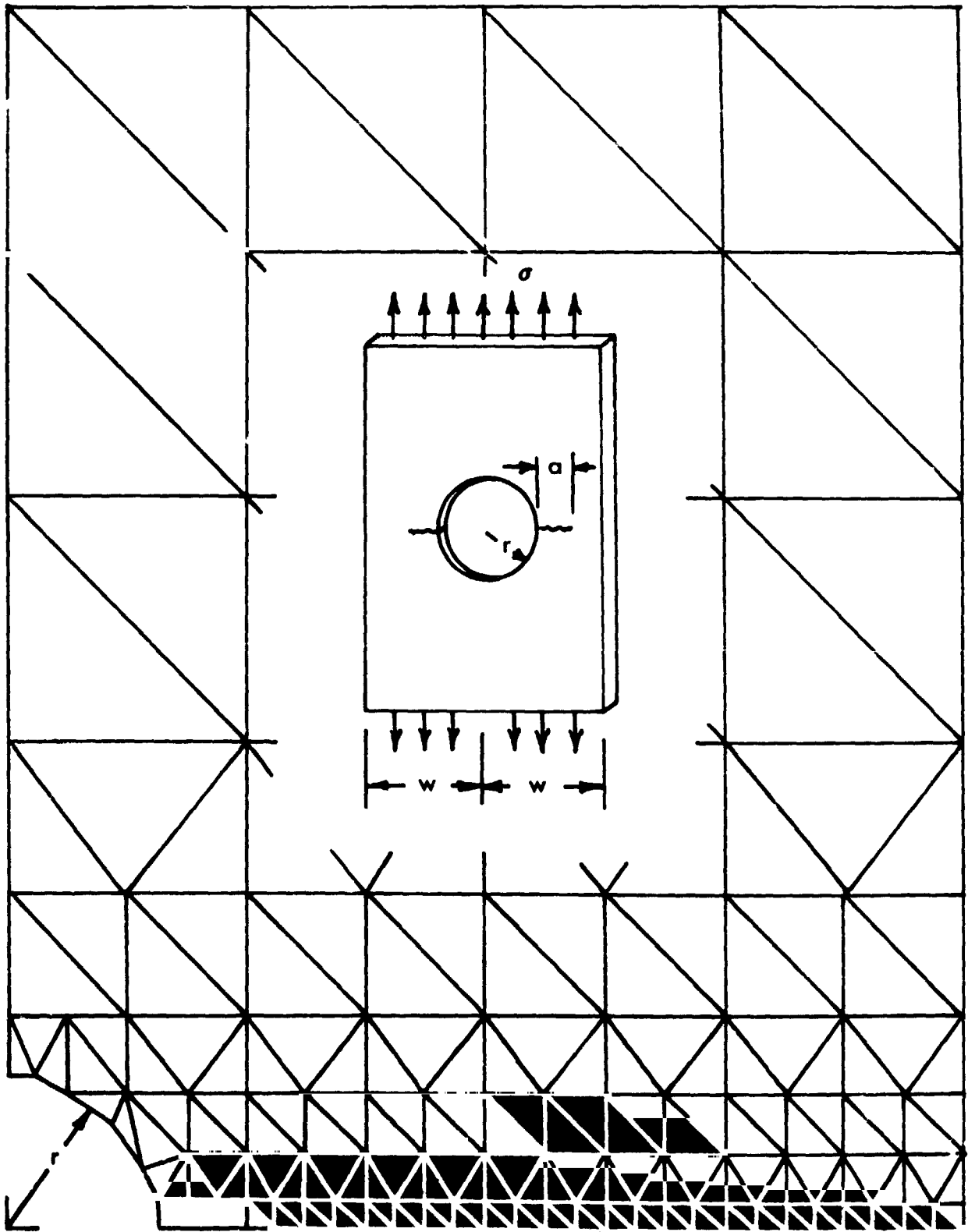


Figure 5.- Symmetric cracks growing from a hole in a finite-width panel.

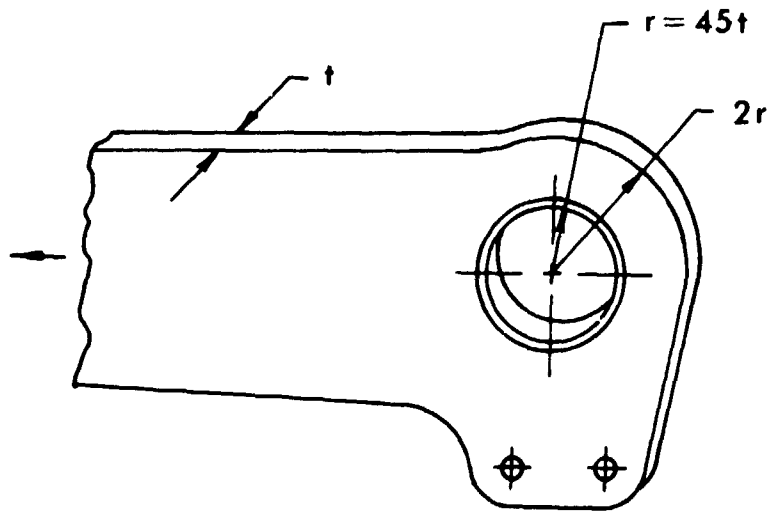


Figure 6.- Lug geometry.

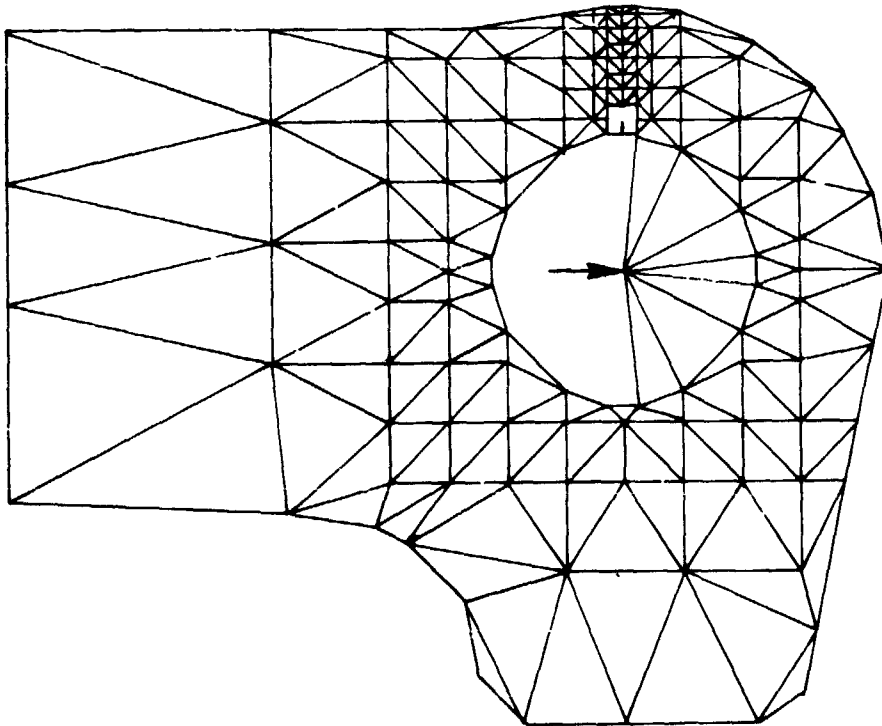


Figure 7.- Finite-element idealization of the lug.

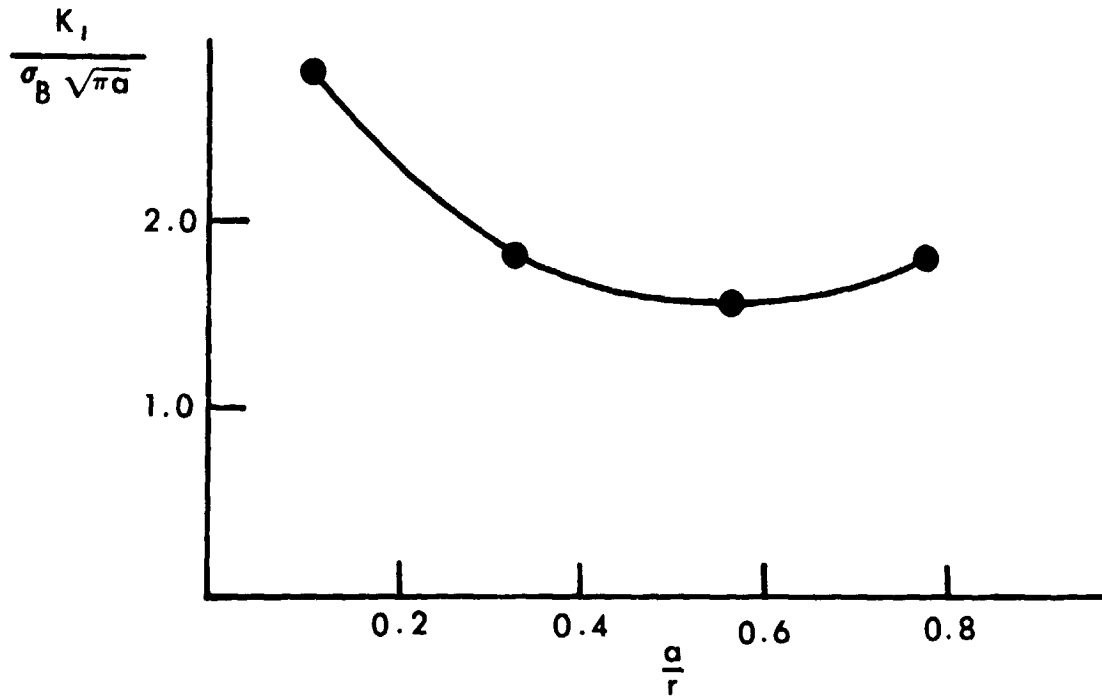


Figure 8.- Stress-intensity factor versus crack length for the lug model.

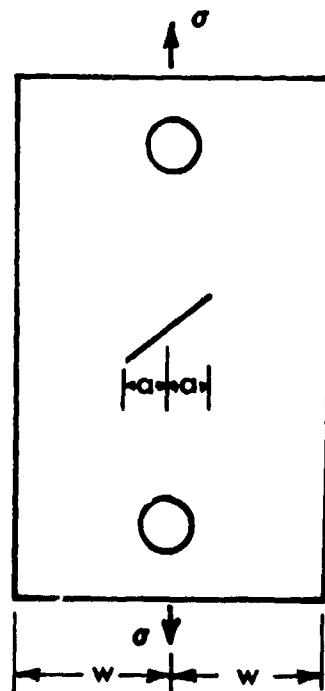


Figure 9.- Tension specimen with a 45° center crack.

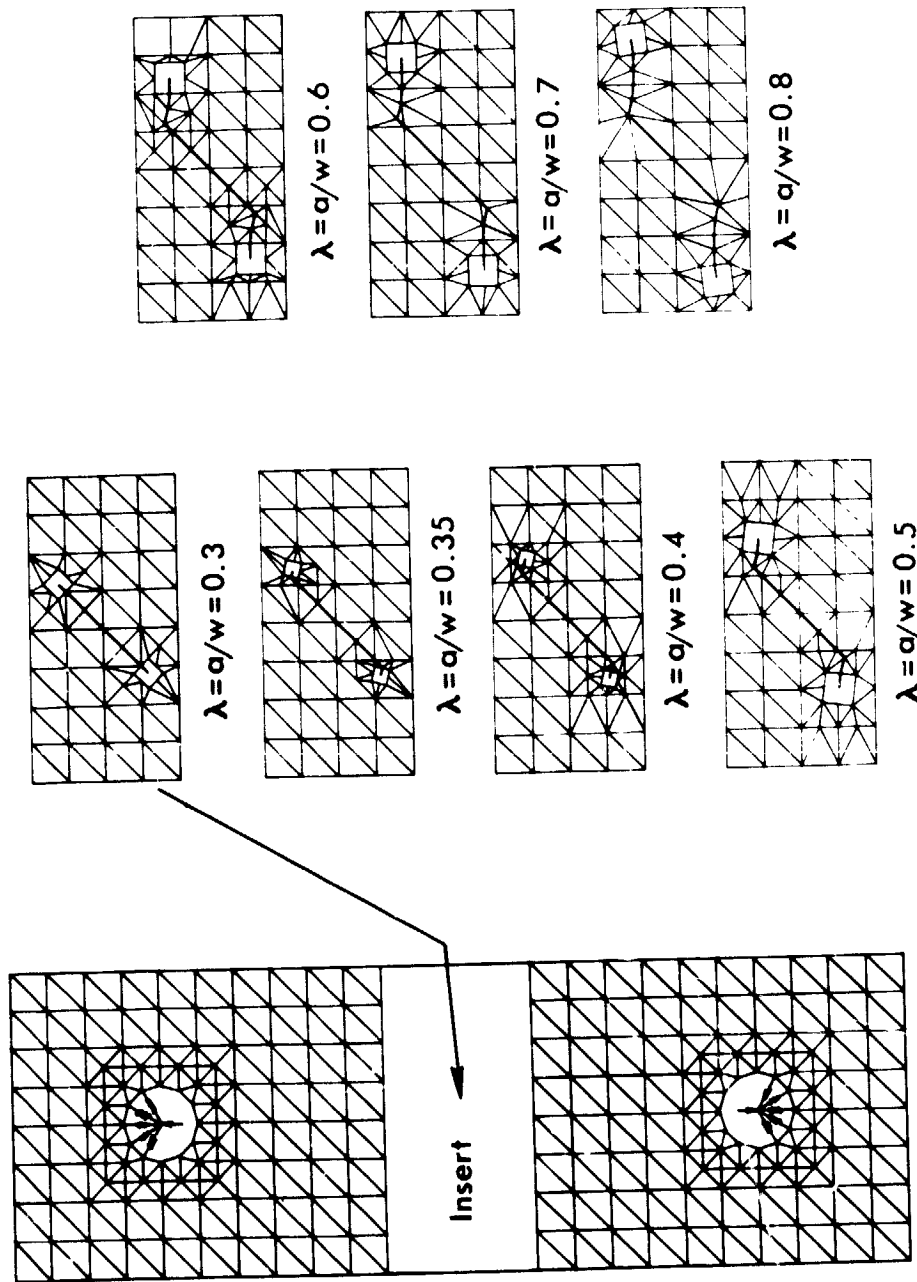


Figure 10. - Finite-element models of tension specimen where initial 45° crack grew experimentally as modeled.

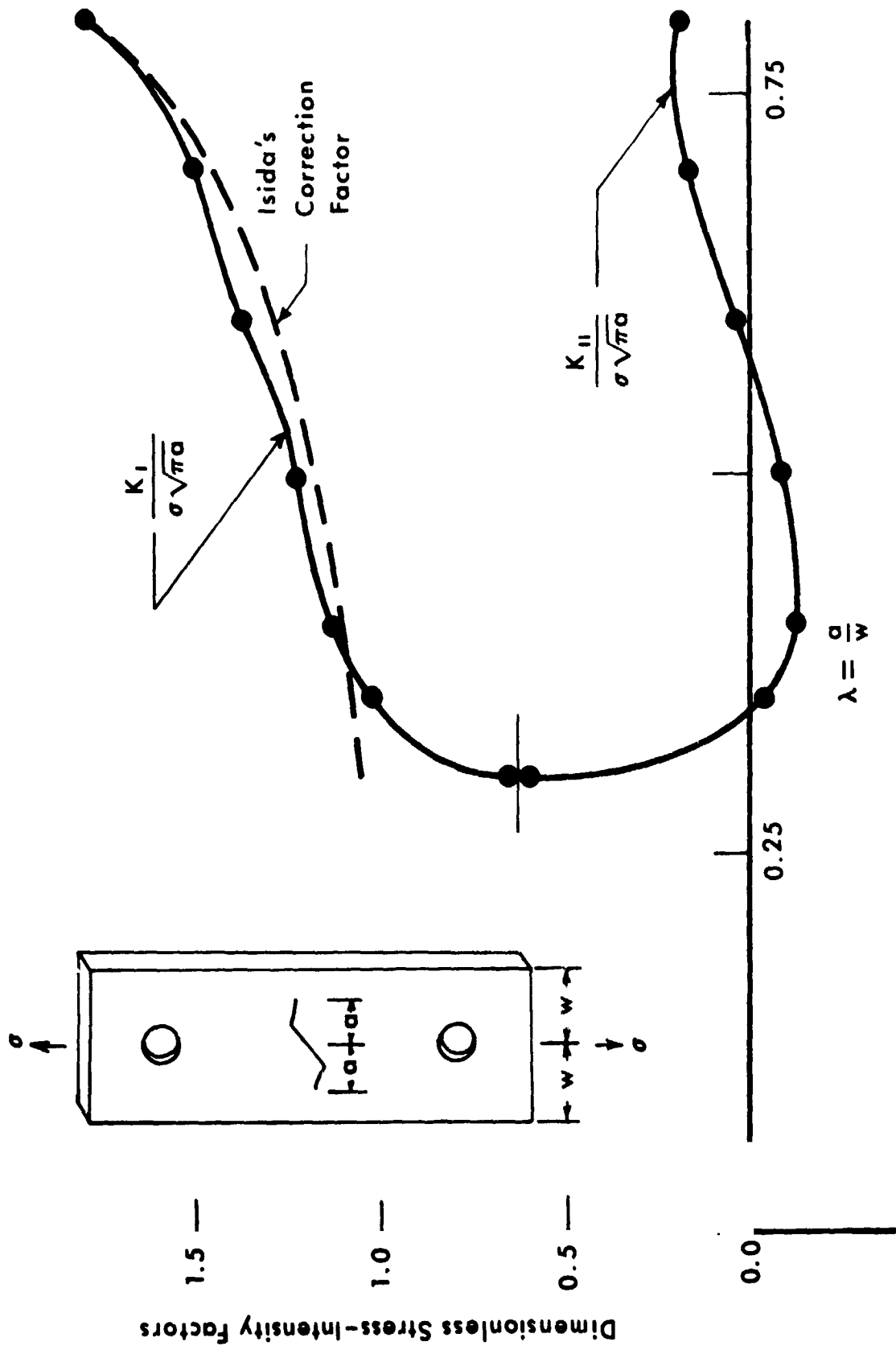


Figure 11. - Stress-intensity factors from the finite-element model shown in figure 10.